analytical chemistry

Article

Cite This: Anal. Chem. XXXX, XXX, XXX−XXX

pubs.acs.org/ac

# Pushing the Resolving Power of Tyndall−Powell Gate Ion Mobility Spectrometry over 100 with No Sensitivity Loss for Multiple Ion Species

Chuang Chen,[†] Hong Chen,[†,‡] and Haiyang Li*[,†]

[†]Key Laboratory of Separation Science for Analytical Chemistry, Dalian Institute of Chemical Physics, Chinese Academy of Sciences, Dalian 116023, People's Republic of China

[‡]University of Chinese Academy of Sciences, Beijing 100039, People's Republic of China

Supporting Information

**ABSTRACT:** Ion gate is a key buildup for drift tube ion mobility spectrometry (IMS) and its combination with mass spectrometry. Bradbury−Nielsen gate, as the most commonly used ion gate in IMS, possesses a distinct ion mobility discrimination effect due to its depletion features. This impedes the scaling of the ion gate opening time to improve the separation capability of IMS while keeping its sensitivity for multiple ion species. In this work, a Tyndall−Powell gate (TPG) simply composed of two identical wire grids was used to develop an ion gate with nearly no ion mobility discrimination for IMS. Experimental results showed that the TPG features a gate region where the electric field for opening the gate could be enhanced to effectively solve the ion mobility discrimination problem related to it. Meanwhile, enhancing that electric field enabled the TPG-IMS to keep a resolving power over 106 at 100 °C for ion peak with a signal-to-noise ratio up to 800. With that TPG-IMS, baseline separation of two ion peaks, the hydronium and the acetone monomer peaks with a reduced mobility difference of only 0.04 $cm^2 V^{-1} s^{-1}$, was achieved with no sensitivity loss for the least mobile acetone dimer ions.

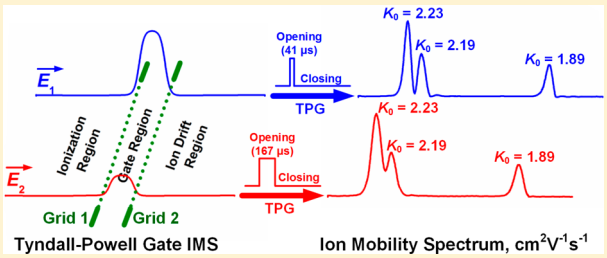


Ion mobility spectrometry (IMS) is a gas-phase ion separation and detection technique, which relies on the ion mobility ($K_0$) differences among ions in low electric field ($E/N$ < 2 Td).[1] It has several main application fields. On one hand, because of its fast separation and high sensitivity features, IMS has been widely employed in portable detection instruments for field screening of narcotics, explosives, chemical warfare agents, etc.[2,3] On the other hand, the relationship between $K_0$ and the ion's collision cross section $\Omega_D$ enables the IMS to do molecular conformational analysis.[4,5] That promotes the use of IMS coupled with MS in biochemistry field to analyze the structure of proteins. Additionally, IMS is also widely used as an additional separation dimension to MS or GC−MS systems.[1]

The principle of IMS mainly consists in two processes: ionization of the sample in the ionization region and separation of the product ions on the basis of their $K_0$ difference in the drift region. For drift tube IMS, narrow ion slices are generated and then travel down the drift region in an electric field. The production of such ion slices is usually achieved with an ion gate placed between the ionization region and the drift region, allowing the ions to pass through in a very short time during one operational period.

As a key element in the IMS design, the ion gate's performance affects the resolving power and the sensitivity of IMS.[6−9] Ideally, the ion gate should have a negligible effective cutting width,[6] allowing equal permeability for all ions. If the detector of IMS is sensitive enough to detect a small slice of ions, the ion gate can be opened for a minimal amount of time to maximize the resolving power.[10,11] When the effective cutting width is not negligible, ions must traverse the cutting width first before entering the drift region in the ion gate opening interval. Any ions lying in the cutting width will be annihilated when the ion gate is closed. For multiple ion species, the ion gate must open for a sufficient amount of time that ensures the least mobile ions to pass through. In turn, the resolving power for the most mobile ions will drop significantly as a result of the longer ion gate open time. High resolving power for the most mobile ions will sacrifice the sensitivity for the least mobile ions, or high sensitivity for the least mobile ions will sacrifice the resolving power for the most mobile ions. That contradiction between resolving power and sensitivity is the so-called ion mobility discrimination effect[6,12] of the ion gate. It is a major concern of IMS researchers trying to improve the separation capability of IMS while keeping its sensitivity for multiple ion species.

The Bradbury−Nielsen gate[12] (BNG) is the most commonly used ion gate in IMS. It usually consists of two sets of parallel wires in one plane.[13−17] As the wires used for making BNG are

Received: September 5, 2017
Accepted: November 18, 2017




DOI: 10.1021/acs.analchem.7b03629
Anal. Chem. XXXX, XXX, XXX−XXX

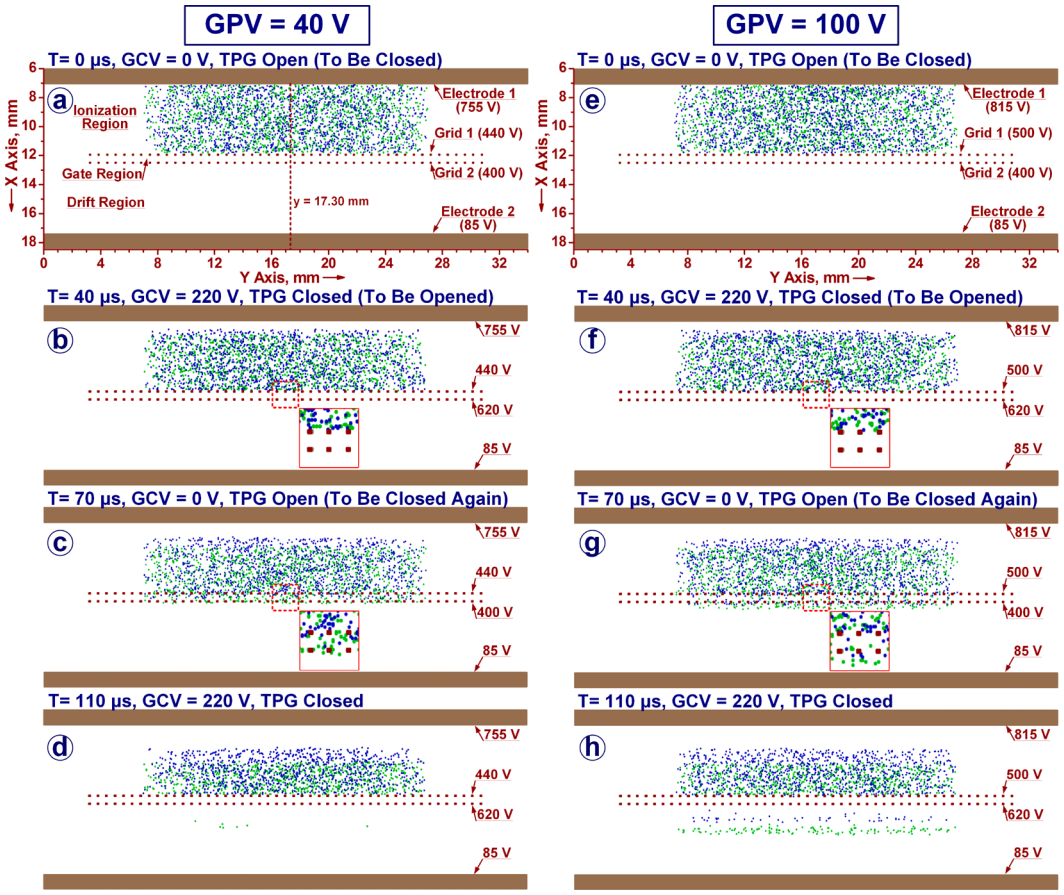


**Figure 1.** SIMION simulation of the ion movement behaviors around the TPG at different GPVs (40 V, left column; 100 V, right column) under 100 °C. The distribution profiles of 1500 ammonia ions ($(NH_3)H^+$, green dots) and 1500 acetone monomer ions ($(CH_3COCH_3)H^+$, blue dots) at four timing points were recorded: the timing start point when the TPG was about to change from open to closed ($t$ = 0 $\mu$s, GCV = 0 V), the TPG closed for the next 40 $\mu$s ($t$ = 40 $\mu$s, GCV = 220 V), the TPG reopened for the next 30 $\mu$s ($t$ = 70 $\mu$s, GCV = 0 V), and the TPG reclosed for the next 40 $\mu$s ($t$ = 110 $\mu$s, GCV = 220 V). GPV stands for the gate penetration voltage defined as the voltage difference between the two grids of the TPG at open status, while GCV stands for the gate closing voltage defined as the extra voltage superposed on the original potential of Grid 2 for closing the TPG.

usually less than 0.1 mm in diameter, BNG shows a negligible geometrical thickness in the ion drift direction. It is widely considered as an ideal ion gate design with equal permeability for multiple ion species. Recent studies,[18−21] however, revealed that there are depletion zones existing on both sides of the BNG plane when it is closed, as a result of the BNG closing electric field penetrating into the ionization and the drift regions. The average thickness of the depletion zones along the ion drift direction is comparable to the wire spacing, around 1 mm thick for a wire spacing of 1 mm.[18,22,23] For a given BNG, as the minimum effective gate closing voltage increases linearly with the ion drift field,[6,8,24] the sizes of the depletion zones stay constant. Thus, increasing the ion drift field has a very limited effect on reducing the ion mobility discrimination effect. Specifically, that discrimination effect becomes more pronounced when the BNG is used in miniaturized IMS drift tubes where a short ion gate opening time is required.

Field switching gate (FSG) is a less commonly used ion gate for IMS.[24,25] In the FSG, a metallic grid is used to separate the ionization chamber from the drift region. The ionization chamber is a narrow field-free region where the ion source lies and the ion population is allowed to build up. In the gate opening interval, a strong field is switched on inside the ionization chamber to inject all of the ions into the drift region. This gate design exhibits nearly no ion mobility discrimination and allows a very short gate opening time for achieving resolving power over 100. The FSG, however, does not fit ion sources of long ionization path such as UV photoionization and corona discharge due to its constrained physical structure.

Tyndall−Powell gate[26,27] (TPG) is another traditional ion gate in IMS. It could be easily crafted with two identical wire or mesh grids in parallel planes.[8,28,29] The two grids are separated by an insulator of 0.5−1 mm thick, forming a gate region that connects the ionization region to the drift region. By switching the potential on either grid of the TPG, a retarding field opposite to the ion drift direction is built inside the gate region to stop ions from going through. The TPG is high temperature tolerant and simpler to craft than the BNG, making it suitable for building robust IMS drift tubes, especially miniaturized ones.[8] However, due to its obvious geometrical thickness along the ion drift direction, the TPG is usually considered as poor permeability for multiple ion species and not suitable for producing narrow ion slices to achieve high resolving power.[1,20] In our recent study, it was found that the two-grid structure of the TPG offers a way to manipulate the penetration behavior of ions going through the TPG, which dramatically changes its performance.


DOI: 10.1021/acs.analchem.7b03629
Anal. Chem. XXXX, XXX, XXX−XXX

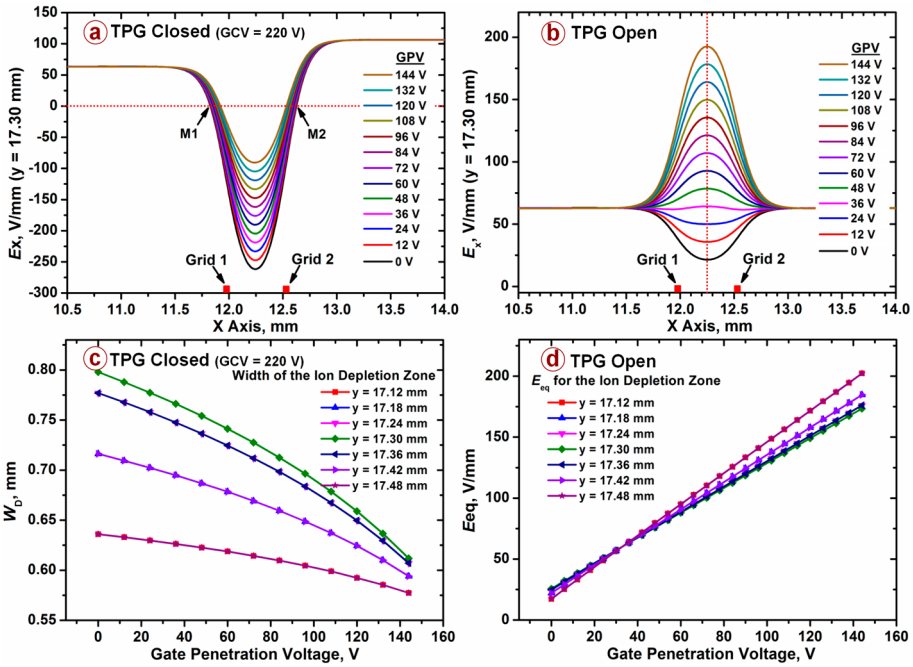


**Figure 2.** Plots of $E_x$ versus $x$ with varying the GPV from 0 to 144 V along $y$ = 17.30 mm when (a) the TPG was open and (b) the TPG was closed. (c) Evolutions of the width of the ion depletion zone $W_D$ along seven $y$ lines with varying the GPV from 0 to 144 V when the TPG was closed. (d) Evolutions of the equivalent electric field $E_{eq}$ for the ion depletion zone along seven $y$ lines with varying the GPV from 0 to 144 V when the TPG was open.

The aim of this work is using TPG to develop an ion gate with nearly no ion mobility discrimination for IMS to achieve high resolving power for multiple ion species. For that purpose, the penetration behavior of ions going through the TPG was explored with SIMION simulation first. It was found that the TPG features a gate region where the electric field for opening the gate could be enhanced to solve the ion mobility discrimination problem related to it. On that base, the experimental performance of the TPG for eliminating the ion mobility discrimination effect and achieving high resolving power in IMS was demonstrated.

## SIMION SIMULATION OF IONS MOVING THROUGH THE TYNDALL–POWELL GATE

The penetration behavior of ions going through the TPG was first explored using the SDS model of SIMION simulation at 100 °C. The geometry of the IMS drift tube is simplified as displayed in Figure 1a. Two 0.94 mm-thick circular electrodes, Electrode 1 and Electrode 2, are positioned in parallel at $x$ = 6.00 mm and $x$ = 17.56 mm, defining a space resembling the IMS drift tube. A TPG comprised of two 0.06 mm-thick grids, Grid 1 and Grid 2, is positioned in the middle of the two electrodes, separating the space into three regions: the ionization, the gate, and the drift regions. The grids are placed in parallel at $x$ = 11.94 mm and $x$ = 12.50 mm, keeping a grid-to-grid distance of 0.5 mm. The two grids are identical wire grids, having parallel square wires with side length of 0.06 mm and wire-to-wire distances of 0.60 mm center-to-center, as used in our following experiments.

At the TPG open status, potentials of 755, 440, 400, and 85 V are applied to Electrode 1, Grid 1, Grid 2, and Electrode 2, forming an electric field of 63 V/mm along the $x$ direction in the ionization and the drift regions. As the potential on Grid 1 is higher than that on Grid 2, the $x$-component of the electric field $E_x$ ($E_x = -dV/dx$) in the gate region is along the $x$ direction ($E_x > 0$), allowing positive ions to go through the TPG (Figure S-1). To close the TPG, the potentials on Electrode 1, Grid 1, and Electrode 2 are kept unchanged. By superposing an extra voltage of 220 V on the original potential (400 V) of Grid 2, the direction of the $E_x$ in the gate region is reversed ($E_x < 0$). The gate region is wholly turned into an ion depletion zone, preventing positive ions from going through the TPG (Figure S-1). At the TPG open status, the potential difference between Grid 1 and Grid 2 is defined as the gate penetration voltage (GPV). To vary the GPV, the potentials on Grid 2 and Electrode 2 are fixed at 400 and 85 V, and the potentials on Electrode 1 and Grid 1 are adjusted simultaneously to keep their difference at 315 V. Additionally, the extra voltage superposed on Grid 2 for closing the TPG is defined as the gate closing voltage (GCV). The GCV is fixed at 220 V for all cases.

To study how ions would move around of the TPG during the gate opening and closing intervals, the GPV is initially set at 40 V. At timing start point $t$ = 0 $\mu$s when the TPG is about to change from open to close, 1500 ammonia ions ($(NH_3)H^+$ with SIMION estimated $K_0$ of 3.6 $cm^2\ V^{-1}\ s^{-1}$, green dots) and 1500 acetone monomer ions ($(CH_3COCH_3)H^+$ with SIMION estimated $K_0$ of 2.3 $cm^2\ V^{-1}\ s^{-1}$, blue dots) randomly distributed in a cylindrical volume of 20 mm in diameter and 5 mm in length are generated at the center of the ionization region, as shown in Figure 1a. Next, the TPG closes for the next 40 $\mu$s while the ions are moving. At timing point $t$ = 40 $\mu$s (Figure 1b), the trailing edges of the two ion packets move away from their origin. Also, the bigger $K_0$ of the ammonia ions enables them to drift farther than the acetone monomer ions. The leading edges, however, both stay at the plane of Grid 1. Actually, part of the ions in the leading edges are deflected onto the Grid 1 wires by the ion depletion zone. Thus, in the TPG reopening period of the next 30 $\mu$s, only ions pass the ion depletion zone would be able to enter the drift region. At


DOI: 10.1021/acs.analchem.7b03629
Anal. Chem. XXXX, XXX, XXX–XXX

timing point $t$ = 70 $\mu$s (Figure 1c), a few ammonia ions already pass the gate region, while the leading edge of the acetone monomer ion packet is still moving in the gate region, just lying in the ion depletion zone. These ions lying in the ion depletion zone would be depleted onto the Grid 1 wires in the TPG reclosing period of the next 40 $\mu$s. As Figure 1d displayed, at timing point $t$ = 110 $\mu$s, the trailing edges are still moving forward, but the leading edges are again stopped at the plane of Grid 1. Meanwhile, only several ammonia ions are drifting in the drift region.

Interestingly, when use a higher GPV of 100 V to repeat the simulation as described above, a very different ion penetration behavior is observed. As shown in Figure 1g, at timing point $t$ = 70 $\mu$s, the leading edges both already pass the gate region after the TPG reopening period of 30 $\mu$s. As a result, ammonia ions and acetone monomer ions drifting in the drift region are observed after the TPG reclosing period of 40 $\mu$s, as Figure 1h displayed. Moreover, the amount of the ammonia ions in the drift region is obviously more than before.

To understand why the ions behave differently at different GPVs, the $E_x$ values in the vicinity of the TPG at closed and open statuses are recorded while varying the GPV from 0 to 144 V. Figure 2a displays the $E_x$ versus $x$ plots at the TPG closed status along $y$ = 17.30 mm, right through the center of the gap between two adjacent grid wires as marked in Figure 1a. The plots overlap in the ionization and the drift regions. Also, each plot has two crossing points, $M_1$ and $M_2$, with the $E_x$ = 0 line. Actually, the distance between $M_1$ and $M_2$ in the $x$ direction reflects the width of the ion depletion zone along $y$ = 17.30 mm, as the $E_x$ values between $M_1$ and $M_2$ are below 0. The calculated width of the ion depletion zone $W_D$ along $y$ = 17.30 mm as varying the GPV from 0 to 144 V is plotted in Figure 2c. As displayed, the $W_D$ decreases as the GPV goes up. This holds true for all of the other six $y$ lines, implying the narrowing of the whole ion depletion zone in the $x$ direction as increasing the GPV. Figure 2b displays the $E_x$ versus $x$ plots along $y$ = 17.30 mm at the TPG open status. The plots overlap in the ionization and the drift regions but vary from low to high levels in the vicinity of the TPG. Using the $E_x$ values on each plot, the equivalent electric field $E_{eq}$ for the ion depletion zone as varying the GPV from 0 to 144 V at the TPG open status is calculated and plotted in Figure 2d. Obviously, the $E_{eq}$ goes up as the GPV goes up along $y$ = 17.30 mm, as well as all of the other six $y$ lines, implying the enhancing of the $E_{eq}$ for the whole ion depletion zone as increasing the GPV at the TPG open status.

As increasing the GPV helps decrease the $W_D$ and increase the $E_{eq}$ for the whole ion depletion zone along the $x$ direction, the time for the same ions to penetrate through the TPG will decrease as the GPV increases as well as the difference between the times for different ion species, which directly reduces the ion mobility discrimination effect of the TPG. Thereby, the ion penetration behaviors displayed in Figure 1 are explained.

## EXPERIMENTAL SECTION

The ion mobility spectrometer used for this work was constructed at our laboratory, as schematically displayed in Figure 3. The IMS cell comprised a 96.5 mm long drift region, a 20 mm long ionization region, and a cylindrical 10 mCi $^{63}$Ni source. The inner diameters of the ionization and the drift regions were 25 mm. A TPG was used in the IMS cell. It comprised two identical wire grids of 0.06 mm thick separated by a circular Teflon insulator of 0.5 mm thick. The grids were

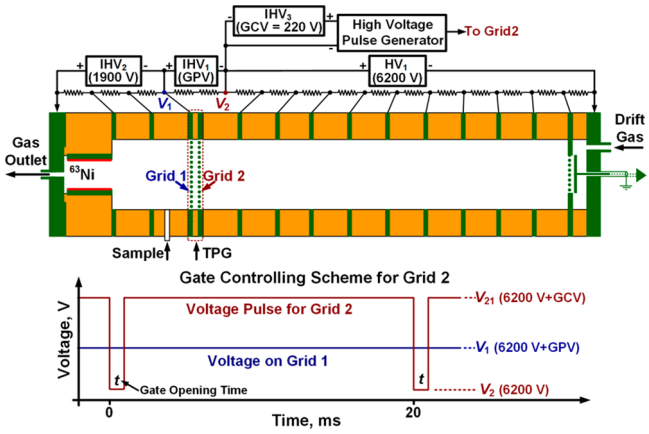


**Figure 3.** Schematic diagram of the Tyndall–Powell gate ion mobility spectrometer (top) and the gate controlling scheme for Grid 2 (bottom). With gate controlling scheme for Grid 2, Grid 1's potential remains at $V_1$, while Grid 2's potential is periodically switched between $V_2$ for opening the gate and $V_{21}$ for closing the gate. The $V_1$ and $V_2$ are the potentials for Grid 1 and Grid 2 at the TPG open status, and their difference is named the gate penetration voltage (GPV). The difference between $V_{21}$ and $V_2$ is named the gate closing voltage (GCV). The GCV is fixed at 220 V for all cases.

made of stainless steel, having parallel square wires with side length of 0.06 mm and a wire-to-wire distance of 0.6 mm center-to-center. The wires spanned a hole of 25 mm diameter on a disc of 40 mm diameter.

A high voltage power supply (HV1) and a serial of 10 MΩ resistors were used to form an electric field of 63 V/mm in the drift region. An isolated high voltage power supply (IHV1) and a serial of 10 MΩ resistors were used to adjust the potential difference between Grid 1 ($V_1$) and Grid 2 ($V_2$) for opening the TPG. That potential difference, $V_1 - V_2$, was defined as the gate penetration voltage (GPV). A second isolated high voltage power supply (IHV2) and a serial of 10 MΩ resistors were used to form an electric field of 63 V/mm in the ionization region. As shown in Figure 3 (bottom), a gate controlling scheme for Grid 2 was used to control the TPG. The voltage pulse for controlling Grid 2 (dark red line) was generated using a high voltage pulse generator (DEI, PVX-4110, U.S.) and a third isolated high voltage power supply (IHV3) floated on the potential ($V_2$) of Grid 2 at the TPG open status. The voltage pulse amplitude ($V_{21} - V_2$) for closing the TPG was defined as the gate closing voltage (GCV). The GCV was fixed at 220 V. The ion current collected by the faraday cup was amplified via a preamplifier of $10^9$ V/A and then recorded by an oscilloscope (Tektronix, 2024C, U.S.). Sixteen times the average was used to obtain each spectrum.

The IMS cell was kept at 100 °C. Ambient air purified by activated carbon, silica gel, and fresh molecular sieves was used as drift and carrier gases at flow rates of 100 and 5 mL min$^{-1}$. The humidity of the air was kept below 1 ppm. The drift and the carrier gases were preheated to 100 °C before entering the drift tube. Acetone and DMMP (dimethyl methyl phosphate) of analytical grade were carried into the IMS by purging a permeation vial (1.5 mL, Agilent). Ammonia produced by self-decomposition of ammonium carbonate was used in the same way. The concentrations of acetone, DMMP, and ammonia were all adjusted high enough (>20 ppm) to react with most of the reactant ions and form a single product ion peak.


DOI: 10.1021/acs.analchem.7b03629
Anal. Chem. XXXX, XXX, XXX–XXX

For safety consideration, a carbon trap was used to trap ammonia, acetone, and DMMP from the gas outlet and prevent environmental pollution. All of the power supplies were operated only by trained personnel.

## RESULTS AND DISCUSSION

**Reduced Ion Mobility Discrimination.** Figure 4 displays the ion mobility spectra obtained with varying the GPV from 6 to 120 V when 5 ppb DMMP was introduced into the acetone doped $^{63}$Ni source. As illustrated, with the GPV fixed at 6 V and the gate opening pulse width (GPW) at 137 $\mu$s, only the acetone dimer peak at 5.67 ms is observed in the spectrum. Prolonging the GPW to 157 $\mu$s, the acetone dimer peak goes up and a DMMP dimer peak of 26.8 pA at 7.53 ms begins to show up in the spectrum. Further increasing the GPW to 229 $\mu$s, the peaks both get stronger. The gradual appearance and going up of the DMMP dimer peak arise from the ion mobility discrimination of the TPG, in which DMMP ions need a longer time to go through the TPG than acetone ions due to its smaller mobility. Obviously, prolonging the GPW allows more DMMP ions to enter the drift region, which helps detect the DMMP dimer ions. However, with varying the GPW from 137 to 229 $\mu$s, more acetone dimer ions are also released into the drift region, causing an obvious decline in its resolving power, from 104 to 54, as listed in Table 1.

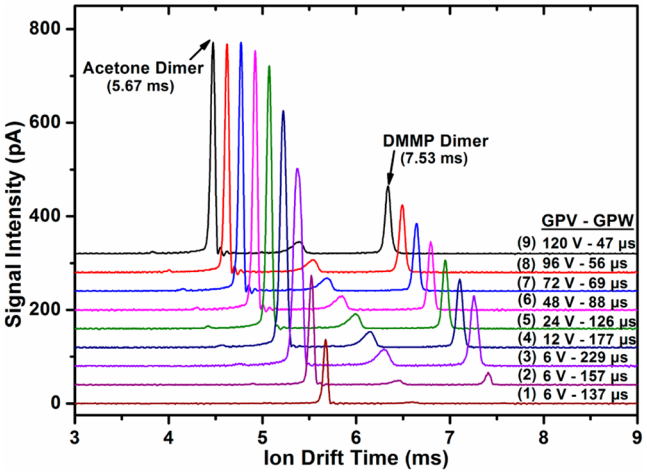


**Figure 4.** Ion mobility spectra obtained with varying the GPV from 6 to 120 V when 5 ppb DMMP was introduced into the acetone doped $^{63}$Ni source. From spectrum 2 to 9, each one was manually shifted with a drift time offset of −0.15 ms relative to the one ahead of it. GPW represents the gate opening pulse width.

On the other hand, the same DMMP dimer peak height as shown in the spectrum at GPV = 6 V and GPW = 229 $\mu$s can also be obtained with shorter GPWs when the GPV is increased. As shown in Figure 4, with the DMMP dimer peak height kept at 144 pA, the GPW decreases from 229 to 47 $\mu$s as the GPV increases from 6 to 120 V. Along with the decrease in the GPW, the peak area ratio of DMMP dimer versus acetone dimer increases from 28% to 44%, implying that the relative amount of DMMP ions versus acetone ions entering the drift region has increased. Meanwhile, the resolving power for the acetone peaks is also enhanced, from 54 to 108, as the GPV increases from 6 to 120 V, which is different from the above case when the GPW is prolonged. These results demonstrate that the ion mobility discrimination effect of the TPG can be effectively reduced by enhancing the GPV. To explain all of this, the effect of the GPV on the gate penetration time (GPT) for ions going through the TPG was first investigated.

**Gate Penetration Time.** Ammonia, acetone dimer, and DMMP dimer ions (Figure S-4) with $K_0$ of 2.60, 1.89, and 1.42 cm$^2$ V$^{-1}$ s$^{-1}$, respectively, were used to study the relationship between the GPT and the GPV. In experimental measurements, the GPT was defined as the minimum GPW for observing a signal with S/N = 3.

The evolutions of the GPT with varying the GPV for the three ions are plotted in Figure 5a. As displayed, the GPT shortens with varying the GPV from 0 to 150 V for all of the ions: for ammonia, it decreases from 91 to 8 $\mu$s; for acetone, it decreases from 121 to 10 $\mu$s; and for DMMP, it decreases from 161 to 13.5 $\mu$s. More interestingly, the GPT differences among the ammonia, acetone dimer, and DMMP dimer ions also shorten with increasing the GPV even though they show distinct $K_0$ differences. As shown in Figure 5b, the GPT difference between DMMP dimer and ammonia ions (with $K_0$ difference of 1.18 cm$^2$ V$^{-1}$ s$^{-1}$) is decreased from 70 $\mu$s at GPV of 0 V to 5.5 $\mu$s at GPV of 150 V, and over 90% of it is eliminated, as so with the other GPT differences. Clearly, the declining of the GPT differences among multiple ion species should be the reason why the ion mobility discrimination effect of the TPG could be reduced by enhancing the GPV as displayed in Figure 4. Considering the ion mobility discrimination effect of an ion gate is actually caused by the GPT differences among ion species with different $K_0$, it is justified to say that a very large amount of the ion mobility discrimination problem related to TPG has been solved in this way.

**Table 1. Detailed Information of the Ion Peaks Shown in Figure 4**

| | | peak area/pA × ms | | | fwhm[a]/$\mu$s | | resolving power[b] | |
|---|---|---|---|---|---|---|---|---|
| GPV/V | GPW/$\mu$s | DMMP | acetone | ratio | DMMP | acetone | DMMP | acetone |
| 6 | 137 | n/a | 8.10 | n/a | n/a | 55 | n/a | 104 |
| 6 | 187 | 1.86 | 15.40 | 12.1% | 68 | 59 | 110 | 89 |
| 6 | 229 | 14.15 | 49.99 | 28.3% | 93 | 105 | 81 | 54 |
| 12 | 177 | 12.37 | 43.40 | 28.5% | 77 | 78 | 98 | 73 |
| 24 | 126 | 11.30 | 38.80 | 28.9% | 72 | 61 | 105 | 94 |
| 48 | 88 | 11.29 | 34.31 | 32.8% | 70 | 55 | 108 | 104 |
| 72 | 69 | 11.27 | 31.63 | 35.6% | 69 | 54 | 109 | 106 |
| 96 | 56 | 11.25 | 28.14 | 40.1% | 68 | 54 | 111 | 107 |
| 120 | 47 | 11.25 | 25.87 | 43.7% | 67 | 53 | 112 | 108 |

[a]fwhm: full width at half-maximum of the ion peak. [b]Resolving power: calculated by the ion peak drift time $t_d$ divided by the fwhm.



DOI: 10.1021/acs.analchem.7b03629
Anal. Chem. XXXX, XXX, XXX−XXX

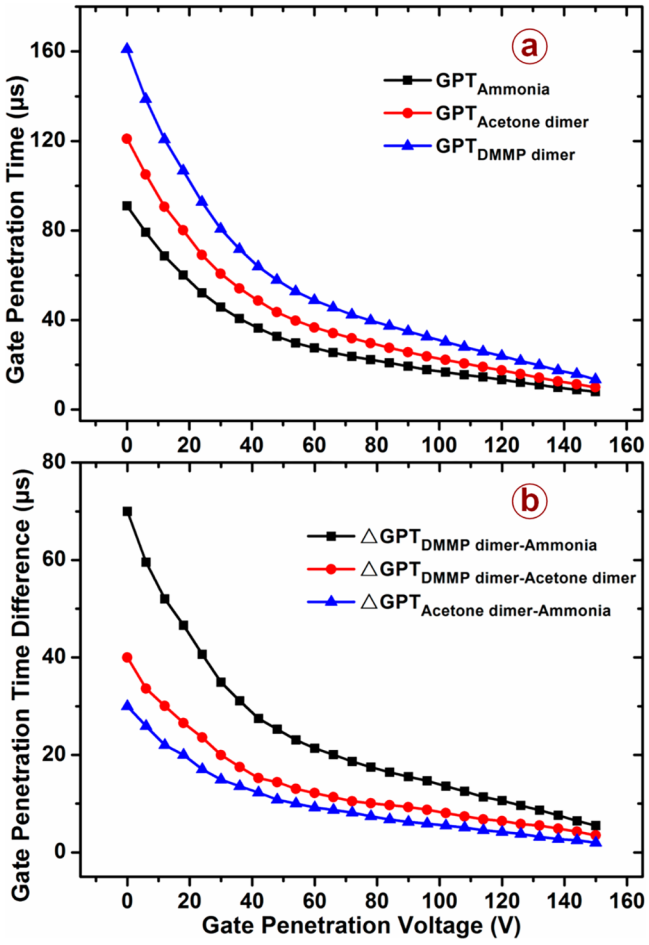


**Figure 5.** (a) Evolutions of the gate penetration time (GPT) with varying the GPV from 0 to 150 V for ammonia, acetone dimer, and DMMP dimer ions, respectively. (b) Evolutions of the gate penetration time difference (ΔGPT) among ammonia, acetone dimer, and DMMP dimer ions with varying the GPV from 0 to 150 V.

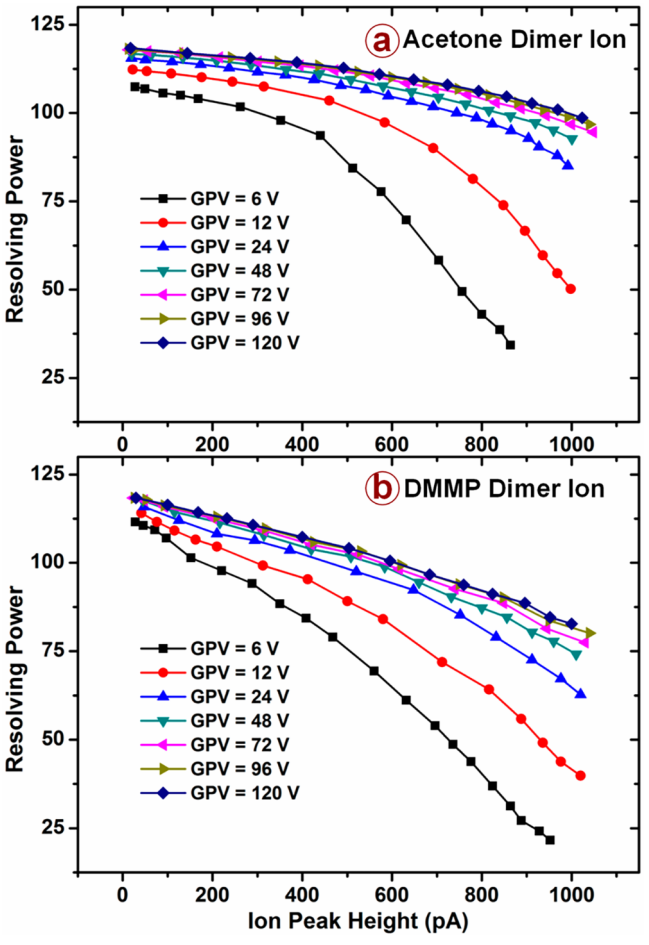


**Figure 6.** Evolutions of the ion peak's resolving power with varying the peak height from 0 to 1000 pA at different GPVs when the $^{63}$Ni source was doped with (a) acetone and (b) DMMP separately.

**Improved Resolving Power.** As shown in Figure 4, increasing the GPV helps reduce the ion mobility discrimination effect, which allows one to apply a narrower GPW to achieve higher resolving power for the acetone dimer ions. Something notable is that the resolving power for the DMMP dimer peak is improved from 81 to 112, even maintaining the same signal intensity. To verify that is not a random phenomenon, evolutions of the resolving power as the ion peak height varying from 0 to 1000 pA at different GPVs were explored when the $^{63}$Ni source was doped with acetone and DMMP separately. The results are plotted in Figure 6.

As Figure 6a displayed, with the acetone dimer peak height kept constant, the resolving power goes up as the GPV increases from 6 to 120 V. For example, at peak height of 200 pA (S/N = 200, baseline noise level is around 1 pA), the resolving power goes from 103 to 116; at 400 pA (S/N = 400), it goes from 95 to 114; and at 800 pA (S/N = 800), it goes from 43 to 106. Similar phenomenon could be observed in Figure 6b where the results for the DMMP dimer peak are exhibited. As the acetone dimer and the DMMP dimer are different ion species, it is believable that the resolving power improving effect of the GPV also applies for other compounds.

To find out the reason behind that, the GPWs for obtaining acetone dimer peak of 400 and 800 pA at different GPVs were measured and listed in Tables S-1 and S-2. As can be seen, with the peak height kept at 400 or 800 pA, the difference between the GPW and the GPT (defined as the effective GPW) reduces as the GPV increases. It means a narrower ion packet is needed to keep the same ion peak height at a higher GPV, which directly results in the resolving power improvement. As varying the GPV does not affect the electric field in the ionization and the drift regions at the TPG open status (Figure 2b), the ion density distribution there would remain unchanged no matter how the GPV varies. We speculate the reduction of the effective GPW may relate to the ion transmission efficiency improvement of the TPG as the GPV increases (Figure S-6). The higher is the ion transmission efficiency, the less is the ion loss on the TPG grids, and, in turn, the narrower the effective GPW would be needed.

**TPG-IMS Separation Capability.** To illustrate the separation power of the new developed TPG-IMS, the separation between hydronium and acetone monomer ions was tested by introducing 5 ppb acetone into the $^{63}$Ni source. As shown in Figure 7, along with the hydronium peak at 4.79 ms ($K_0$ of 2.23 cm$^2$ V$^{-1}$ s$^{-1}$), two product ion peaks show up: one at 4.88 ms ($K_0$ of 2.19 cm$^2$ V$^{-1}$ s$^{-1}$) and the other at 5.67 ms ($K_0$ of 1.89 cm$^2$ V$^{-1}$ s$^{-1}$), corresponding to the acetone monomer and the acetone dimer ions. By increasing the GPV from 6 to 120 V, baseline separation between the hydronium peak and the acetone monomer peak is achieved even though


DOI: 10.1021/acs.analchem.7b03629
Anal. Chem. XXXX, XXX, XXX−XXX

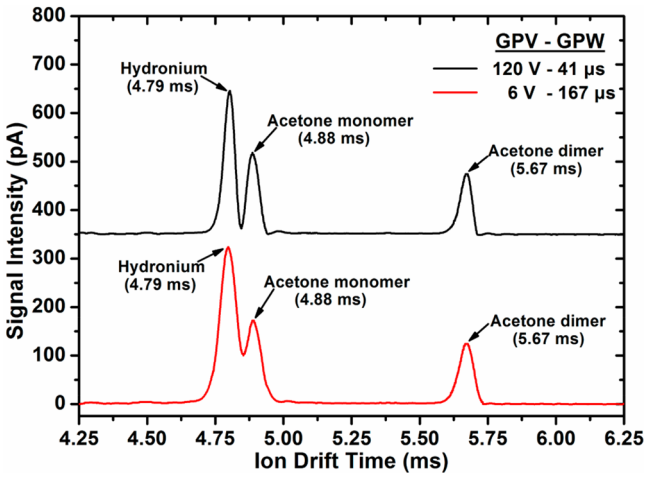


**Figure 7.** Separation of the ion peaks when 5 ppb acetone was introduced into the $^{63}$Ni source.

they show a tiny $K_0$ difference of 0.04 cm$^2$ V$^{-1}$ s$^{-1}$. Meanwhile, the acetone dimer peak height is maintained at 124 pA (S/N = 124) with no sensitivity loss.

## CONCLUSION

Like BNG, TPG is also a traditional ion gate in IMS. They are universally applicable for different ion sources and share the same ion gate controlling circuits. Yet the TPG is much easier to craft than the BNG. Two identical wire or mesh grids placed in parallel will do, and the two grids do not need to be aligned precisely. Its gating performance is usually considered as worse than the BNG due to its thick gate region confined by the two grids. Actually, the two-grid structure offers a way to solve the ion mobility discrimination problem, which is not achievable with the BNG. As demonstrated in this work, by enhancing the electric field in the TPG gate region for opening it, the ion mobility discrimination problem related to TPG was effectively solved. Also, with TPG-IMS, baseline separation between the hydronium and the acetone monomer peaks was achieved without causing sensitivity loss for the least mobile acetone dimer ions. These results may give valuable instructions for IMS researchers to design high performance IMS drift tubes, especially the miniaturized ones.

## ASSOCIATED CONTENT

### Supporting Information

The Supporting Information is available free of charge on the ACS Publications website at DOI: 10.1021/acs.analchem.7b03629.

Additional information as noted in the text (PDF)

## AUTHOR INFORMATION

### Corresponding Author

*Fax: +86-411-84379517. E-mail: hli@dicp.ac.cn.

### ORCID

Haiyang Li: 0000-0002-6658-4745

### Notes

The authors declare no competing financial interest.

## ACKNOWLEDGMENTS

This work was supported by the National Natural Science Foundation of China (Grant no. 21405158) and the Chinese Academy of Sciences Visiting Fellowship for Researchers from Developing Countries (Grant no. 2013FFG0011).

## REFERENCES

(1) Eiceman, G. A.; Karpas, Z.; Hill, H. H. *Ion Mobility Spectrometry*, 3rd ed.; CRC Press: Boca Raton, FL, 2013.
(2) Borsdorf, H.; Mayer, T.; Zarejousheghani, M.; Eiceman, G. A. *Appl. Spectrosc. Rev.* **2011**, *46*, 472−521.
(3) Eiceman, G. A.; Stone, J. A. *Anal. Chem.* **2004**, *76*, 390−397.
(4) Kirk, A. T.; Raddatz, C. R.; Zimmermann, S. *Anal. Chem.* **2017**, *89*, 1509−1515.
(5) Hofmann, J.; Hahm, H. S.; Seeberger, P. H.; Pagel, K. *Nature* **2015**, *526*, 241−244.
(6) Tabrizchi, M.; Shamlouei, H. R. *Int. J. Mass Spectrom.* **2010**, *291*, 67−72.
(7) Tadjimukhamedov, F. K.; Puton, J.; Stone, J. A.; Eiceman, G. A. *Rev. Sci. Instrum.* **2009**, *80*, 103103.
(8) Babis, J. S.; Sperline, R. P.; Knight, A. K.; Jones, D. A.; Gresham, C. A.; Denton, M. B. *Anal. Bioanal. Chem.* **2009**, *395*, 411−419.
(9) Eiceman, G. A.; Nazarov, E. G.; Rodriguez, J. E.; Stone, J. A. *Rev. Sci. Instrum.* **2001**, *72*, 3610.
(10) Kanu, A. B.; Gribb, M. M.; Hill, H. J. *Anal. Chem.* **2008**, *80*, 6610−6619.
(11) Siems, W. F.; Wu, C.; Tarver, E. E.; Hill, H. J.; Larsen, P. R.; McMinn, D. G. *Anal. Chem.* **1994**, *66*, 4195−4201.
(12) Bradbury, N.; Nielsen, R. *Phys. Rev.* **1936**, *49*, 388−393.
(13) Zuleta, I. A.; Barbula, G. K.; Robbins, M. D.; Yoon, O. K.; Zare, R. N. *Anal. Chem.* **2007**, *79*, 9160−9165.
(14) Yoon, O. K.; Zuleta, I. A.; Robbins, M. D.; Barbula, G. K.; Zare, R. N. *J. Am. Soc. Mass Spectrom.* **2007**, *18*, 1901−1908.
(15) Szumlas, A. W.; Rogers, D. A.; Hieftje, G. M. *Rev. Sci. Instrum.* **2005**, *76*, 086108.
(16) Kimmel, J. R.; Engelke, F.; Zare, R. N. *Rev. Sci. Instrum.* **2001**, *72*, 4354.
(17) Salleras, M.; Kalms, A.; Krenkow, A.; Kessler, M.; Goebel, J.; Müller, G.; Marco, S. *Sens. Actuators, B* **2006**, *118*, 338−342.
(18) Du, Y.; Wang, W.; Li, H. *Anal. Chem.* **2012**, *84*, 5700−5707.
(19) Du, Y.; Wang, W.; Li, H. *Anal. Chem.* **2012**, *84*, 1725−1731.
(20) Puton, J.; Knap, A.; Siodłowski, B. *Sens. Actuators, B* **2008**, *135*, 116−121.
(21) Eiceman, G. A.; Vandiver, V. J.; Chen, T.; Rico-Martinez, G. *Instrum. Sci. Technol.* **1989**, *18*, 227−242.
(22) Chen, C.; Tabrizchi, M.; Wang, W.; Li, H. *Anal. Chem.* **2015**, *87*, 7925−7930.
(23) Stoermer, C. W.; Gilb, S.; Friedrich, J.; Schooss, D.; Kappes, M. M. *Rev. Sci. Instrum.* **1998**, *69*, 1661.
(24) Kirk, A. T.; Zimmermann, S. *Int. J. Ion Mobility Spectrom.* **2014**, *17*, 131−137.
(25) Kirk, A. T.; Allers, M.; Cochems, P.; Langejuergen, J.; Zimmermann, S. *Analyst* **2013**, *138*, 5200−5207.
(26) Tyndall, A. M. *The Mobility of Positive Ions in Gases*; Cambridge University Press: Cambridge, UK, 1938.
(27) Tyndall, A. M.; Powell, C. F. *Proc. R. Soc. London, Ser. A* **1930**, *129*, 162−180.
(28) Langejuergen, J.; Allers, M.; Oermann, J.; Kirk, A.; Zimmermann, S. *Anal. Chem.* **2014**, *86*, 7023−7032.
(29) Karpas, Z.; Guaman, A. V.; Pardo, A.; Marco, S. *Anal. Chim. Acta* **2013**, *758*, 122−129.



DOI: 10.1021/acs.analchem.7b03629
*Anal. Chem.* XXXX, XXX, XXX−XXX